Biomaterials Science

PAPER

View Article Online
View Journal | View Issue

Cite this: *Biomater. Sci.*, 2016, **4**, 448

Curcumin loaded mesoporous silica: an effective drug delivery system for cancer treatment†

Rajesh Kotcherlakota,[a] Ayan Kumar Barui,[a,b] Sanjiv Prashar,[c] Mariano Fajardo,[c] David Briones,[d] Antonio Rodríguez-Diéguez,[d] Chitta Ranjan Patra*[a,b] and Santiago Gómez-Ruiz*[c]

Received 25th November 2015,
Accepted 2nd December 2015

DOI: 10.1039/c5bm00552c

www.rsc.org/biomaterialsscience

In the present study, we report the delivery of anti-cancer drug curcumin to cancer cells using mesoporous silica materials. A series of mesoporous silica material based drug delivery systems (**S2**, **S4** and **S6**) were first designed and developed through the amine functionalization of KIT-6, MSU-2 and MCM-41 followed by the loading of curcumin. The curcumin loaded materials were characterized with several physico-chemical techniques and thoroughly screened on cancer cells to evaluate their *in vitro* drug delivery efficacy. All the curcumin loaded silica materials exhibited higher cellular uptake and inhibition of cancer cell viability compared to pristine curcumin. The effective internalization of curcumin in cancer cells through the mesoporous silica materials initiated the generation of intracellular reactive oxygen species and the down regulation of poly ADP ribose polymerase (PARP) enzyme levels compared to free curcumin leading to the activation of apoptosis. This study shows that the anti-cancer activity of curcumin can be potentiated by loading onto mesoporous silica materials. Therefore, we strongly believe that mesoporous silica based curcumin loaded drug delivery systems may have future potential applications for the treatment of cancers.

Introduction

Curcuma longa has extensively been used as a food additive and conservant in India, China and other Asian countries.[1] In addition, it has been used for domestic remediation in Chinese medicine for different diseases such as diabetes, hepatic dysfunctions and other health problems.[2] For this reason, during the last decades a high number of studies have been carried out in order to determine the biological activity and pharmacological properties of *Curcuma longa* and its extracts.[3] Curcumin is the major curcuminoid and the main bioactive component of *Curcuma longa*. It has diverse biological applications as an antioxidant, antimutagenic, antidiabetic, antibacterial, antifungal and especially as an anticancer agent.[4] Curcumin has also been used in clinical trials for the reduction of the inflammatory processes after surgery.[5] Furthermore, earlier reports demonstrate that curcumin is cytotoxic to various cancer cells through the induction of apoptosis and decrease of cell invasiveness of the tumoural area.[6] Dose dependent toxicity studies in normal cell lines suggest that curcumin is well tolerated at high doses without any toxic effect. However, the administration of curcumin in the human body as an anti-cancer agent has not been found to be effective due to its lower systemic bioavailability originating from its low solubility and instability.[7] To overcome these limitations, researchers have been engaged in making different formulations such as the encapsulation of curcumin with polymeric nanoparticles or silicalization of curcumin-loaded solid lipid nanoparticle (SLN)/micelle dispersions,[8] metal or non-metal nanoparticles, phospholipids, microemulsions or by the preparation of other curcumin analogues.[9] Amongst all these approaches, the prevalent one is the encapsulation of curcumin with nanoparticles. However, rigorous studies are still needed to evaluate the efficacy and toxicity of the nanoparticles.[10a,b]

A different approach for developing novel drug-delivery systems is the use of mesoporous silica materials because of their interesting properties, such as (i) variable and controllable particle sizes ranging from 50 nm to microns that lead to an easy endocytosis by cells and possess low cytotoxicity,

[a]*Biomaterials Group, CSIR-Indian Institute of Chemical Technology, Uppal Road, Tarnaka, Hyderabad 500007, India. E-mail: crpatra@iict.res.in, patra.chitta@gmail.com*
[b]*Academy of Scientific and Innovative Research (AcSIR), Training and Development Complex, CSIR Campus, CSIR Road, Taramani, Chennai – 600 113, India*
[c]*Departamento de Biología y Geología, Física y Quimica Inorgánica, E.S.C.E.T., Universidad Rey Juan Carlos, Calle Tulipán s/n, 28933, Móstoles, Madrid, Spain. E-mail: santiago.gomez@urjc.es*
[d]*Departamento de Química Inorgánica, Universidad de Granada, Facultad de Ciencias, Fuente Nueva s/n 18071, Granada, Spain*
†Electronic supplementary information (ESI) available. See DOI: 10.1039/c5bm00552c

(ii) stability to heat, pH, mechanical stress and chemical degradations, (iii) tunable narrow pore size distribution and pore diameter that lead to a rational loading of different drug molecules, (iv) high surface area which allows a good degree of drug incorporation and (v) easy functionalization of the external and internal surface by different ligands, metal complexes, biomaterials or other nanostructures.[10b] For all these reasons, silica-based mesoporous materials have been used as drug delivery vehicles in various biomedical applications, such as anti-inflammatory, analgesic, bone regeneration and also in anti-cancer treatments.[10c–e]

Considering their biomedical applications, the mesoporous silica materials KIT-6, MSU-2 and MCM-41 have been chosen as models with high porosity and capacity of loading of curcumin in order to study their biological behaviour as drug-delivery systems, as a first step before a plausible therapeutic application. In this context, we have synthesized a series of silica based mesoporous materials (KIT-6, MSU-2 and MCM-41, with different particle sizes, pore sizes and morphology), which have been functionalized with 3-aminopropyltriethoxysilane (APTES) to give rise to amine functionalized materials (**S1**, **S3** and **S5**). Further, we have developed **S1**, **S3** and **S5** based drug delivery systems by conjugating them with curcumin, namely **S2**, **S4** and **S6**, respectively. All the materials have been characterized by several physico-chemical techniques such as TEM (transmission electron microscopy), SEM (scanning electron microscopy), FT-IR (Fourier transform infrared spectroscopy), TGA (thermogravimetric analysis) and BET (Brunauer–Emmett–Teller) analysis. Release kinetic studies with the curcumin loaded mesoporous materials (**S2**, **S4** and **S6**) reveal a slow and sustained release of curcumin under physiological conditions (pH: 7.4). The *in vitro* cell culture study of the synthesized materials shows that all of them are biocompatible for normal cell lines (NIH-3T3 and CHO). However, the curcumin loaded mesoporous silica materials, especially **S4**, are found to be cytotoxic towards different cancer cells (A549, MCF-7 and SKOV3) compared to free curcumin. The generation of intracellular ROS ($O_2^{\bullet-}$) and the down regulation of PARP expression levels leading to the activation of apoptosis have been found to be the molecular mechanisms behind the anticancer potential of curcumin loaded mesoporous silica materials. In addition, although some studies using APTES as an immobilizing agent have been previously reported, no materials have been published to date with the combination of APTES–curcumin and all the spectroscopic and biological data of the final materials **S2**, **S4** and **S6** are new. These results show the future potential applications of mesoporous silica-based materials as drug delivery systems for the treatment of several tumours.

Experimental section

Chemistry

General remarks on the synthesis of the materials. The synthesis of the materials was performed under dry nitrogen gas using standard Schlenk techniques and a dry box. Solvents were distilled from the appropriate drying agents and degassed before use. Tetraethyl orthosilicate (TEOS) 98% (MW = 208.33, d = 0.934 g mL^{-1}), dodecylamine (DDA) 98% (M = 185.36), poly(ethylene glycol)-*block*-poly(propylene glycol)-*block*-poly-(ethylene glycol) (M_{av} = 5800; d = 1.019 g mL^{-1}) and Tergitol® NP-9 (MW = 616.82) were purchased from Sigma-Aldrich and were used without further purification. Water (resistance 18.2 MΩ cm) used in the preparation of materials was obtained from a Millipore Milli-Q-System (Billerica, MA, USA). Curcumin (95% purity) was purchased from Alfa Aesar and used without further purification.

General remarks on the characterization of the materials. ^{1}H MAS NMR (4 μs 90° pulse, spinning speed of 9 MHz, pulse delay 2 s), ^{13}C-CP MAS NMR (4.40 μs 90° pulse, spinning speed of 6 MHz, pulse delay 2 s) and ^{29}Si MAS NMR (8 μs 90° pDa, spinning speed of 6 MHz, pulse delay 10 s) spectra, were recorded on a Varian-Infinity Plus Spectrometer at 400 MHz operating at 100.52 MHz proton frequency. X-ray diffraction (XRD) patterns of the silicas were obtained on a Philips Diffractometer model PW3040/00 X'Pert MPD/MRD at 45 KV and 40 mA, using wavelength Cu Kα (λ = 1.5418 Å). IR spectra were recorded on a Thermo Nicolet Avatar 330 FTIR spectrophotometer pressing *ca.* 1 mg of material on a ZnSe crystal at 11 psi. The thermal stability of the modified mesoporous silicas was studied using a Setsys 18 A (Setaram) thermogravimetric analyzer and a platinum crucible of 100 μL. A synthetic air atmosphere was used and the temperature increased from 25 °C to 800 °C at a speed of 5 °C per min. N_2 gas adsorption–desorption study was performed using a Micromeritics ASAP 2020 analyzer. Scanning electron micrographs and the morphological analysis were carried out on a XL30 ESEM Philips with an energy dispersive spectrometry system (EDS). The samples were treated with a sputtering method with the following parameters: sputter time 100 s, sputter current 30 mA, film thickness 20 nm using a sputter coater BAL-TEC SCD 005. Conventional transmission electron microscopy (TEM) was carried out on a TECNAI 20 Philips, operating at 200 kV. SEM images were taken in solid state (without any previous dispersion step) and TEM images were taken just after a very short dispersion in acetone and ultrasounds (to prevent the release of curcumin) and subsequent vacuum treatment, so aggregates of particles are very common when analysing the systems in the solid state.

Preparation of template materials

Preparation of KIT-6. The large pore 3D (*Ia3d*) cubic silica mesostructure, designated as KIT-6, was prepared using Pluronic P123 ($EO_{20}PO_{70}EO_{20}$) template as a structure directing agent and tetraethyl orthosilicate (TEOS) as the silica precursor according to the previous report.[11] In a typical synthesis, 30 g (5.15 mmol) of P123 and 30 g of *n*-butanol (0.905 mol) were mixed with 1350 g (75 mol) of distilled water and 57.0 g (0.575 mol) of concentrated hydrochloric acid (37 wt% HCl). To this mixture, 64.5 g (0.305 mol) of TEOS were added. The mixture was then stirred at 45 °C for 24 hours to allow the formation of the mesostructured product. Subsequently, the

reaction mixture was heated for 24 hours at 95 °C under static conditions for hydrothermal treatment. The solid product was then filtered, washed several times with deionized water and dried at 100 °C. Finally, the sample was calcined at 550 °C for 48 hours to remove the template. Textural properties: S_{BET}: 700 $m^2\ g^{-1}$. V_p: 0.60 $cm^3\ g^{-1}$. d_p: 76.2 Å.

Preparation of MSU-2. A mesoporous silica of the MSU-X family (MSU-2-type) was prepared using the synthetic method reported previously.[12] MSU-2 was synthesized by a two-step process: firstly TEOS was added to a stirring 0.08 M (pH 4.8) solution of Tergitol® NP-9 in Milli-Q water at room temperature to obtain a milky suspension (TEOS–surfactant solution molar ratio of 8/1). The resulting suspension was then aged without agitation for 20 hours to give a clear solution. In the second step, a 0.24 M sodium fluoride solution was added drop wise with stirring to the TEOS–surfactant solution to obtain a NaF/TEOS molar ratio of 0.025/1. The solution were placed in a bath with agitation at 55 °C for 48 hours. The final product was filtered off, washed with Milli-Q water and air-dried at 100 °C for 4 hours. Finally, the surfactant was removed by calcination in air at 600 °C for 12 hours. The surface was then dehydrated under vacuum (10^{-2} mmHg) for 16 hours at 250 °C, cooled and stored under dry nitrogen. Textural properties: S_{BET}: 843 $m^2\ g^{-1}$; V_p: 0.97 $cm^3\ g^{-1}$; d_p: 51.1 Å.

Preparation of MCM-41. MCM-41 was prepared according to the method of Landau *et al.* using hydrothermal synthesis.[13] The material was subsequently dehydrated under vacuum (10^{-2} mmHg) for 16 hours at 200 °C, cooled and stored under dry nitrogen. Textural properties: S_{BET}: 1117 $m^2\ g^{-1}$; V_p: 1.12 $cm^3\ g^{-1}$; d_p: 29.6 Å.

Preparation of amine functionalized materials

Preparation of S1 (KIT-6-AP). A solution of 3-aminopropyltriethoxysilane (5.80 mL, 22.6 mmol) in toluene (100 mL) was added to dehydrated KIT-6 (5.00 g) and the mixture was stirred for 48 hours at 100 °C. The slurry was filtered through fritted discs and the solid residue was washed with toluene (5 × 200 mL), ethanol (5 × 200 mL), methanol (5 × 200 mL) and diethyl ether (5 × 200 mL). The resultant solid was dried under vacuum at room temperature for 24 hours to obtain a white free flowing powder. Textural properties: S_{BET}: 130 $m^2\ g^{-1}$; V_p: 0.20 $cm^3\ g^{-1}$; d_p: 62.5 Å.

Preparation of S3 (MSU-2-AP). S3 was prepared using the same procedure for the preparation of **S1**. 3-Aminopropyltriethoxysilane (5.80 mL, 22.6 mmol) in toluene (100 mL), MSU-2 (5.00 g). Textural properties: S_{BET}: 470 $m^2\ g^{-1}$; V_p: 0.67 $cm^3\ g^{-1}$; d_p: 39.5 Å.

Preparation of S5 (MCM-41-AP). S5 was prepared using the same procedure for the preparation of **S1**. 3-Aminopropyltriethoxysilane (5.80 mL, 22.6 mmol) in toluene (100 mL), MCM-41 (5.00 g). Textural properties: S_{BET}: 650 $m^2\ g^{-1}$; V_p: 0.25 $cm^3\ g^{-1}$; d_p: 18.3 Å.

Preparation of curcumin loaded materials

Preparation of S2 (KIT-6-AP-CUR). A solution of curcumin (0.63 g, 2.40 mmol) (to obtain a theoretical level of 20% curcumin/**S1**) in ethanol (100 mL) was added to **S1** (2.50 g) and the mixture was stirred under reflux conditions for 48 hours. The slurry was filtered through fritted discs and the solid residue was dried under vacuum at room temperature for 24 hours to give a pale orange free flowing powder. Textural properties: S_{BET}: 20 $m^2\ g^{-1}$; V_p: 0.04 $cm^3\ g^{-1}$; d_p: <18 Å.

Preparation of S4 (MSU-2-AP-CUR). S4 was prepared using the same procedure for the preparation of **S2**. Curcumin (0.63 g, 2.40 mmol) (to obtain a theoretical level of 20% curcumin/**S3**) in ethanol (100 mL) and **S3** (2.50 g). Textural properties: S_{BET}: 425 $m^2\ g^{-1}$; V_p: 0.49 $cm^3\ g^{-1}$; d_p: 35.4 Å.

Preparation of S6 (MCM-41-AP-CUR). S6 was prepared using the same procedure for the preparation of **S2**. Curcumin (0.63 g, 2.40 mmol) (to obtain a theoretical level of 20% curcumin/**S5**) in ethanol (100 mL) and **S5** (2.50 g). Textural properties: S_{BET}: 414 $m^2\ g^{-1}$; V_p: 0.17 $cm^3\ g^{-1}$; d_p: <18 Å.

Release studies in biological conditions

The curcumin release from the materials in biological conditions was carried out in a blood simulated fluid (tris buffer: pH 7.4).[14a] 5 mL of the mixture of aqueous buffer : ethanol (95 : 5; v/v) was added to 10 mg of the studied materials. These suspensions were incubated at 37 °C in a water bath for different time periods up to 240 hours. The suspension was then centrifuged and filtered through a nylon filter (0.45 μm) and the filtrate was diluted to the working concentration with ethanol. The quantification of the curcumin was immediately carried out measuring the absorbance of the solutions using UV-Visible spectroscopy at λ_{max} of 428 nm.

Biology

Materials and methods. Dulbecco's modified eagle medium (DMEM), Dulbecco's phosphate buffered saline (DPBS), fetal bovine serum (FBS), penicillin/streptomycin, dihydroethidium (DHE), propidium iodide, Hoechst-33258 and BCIP–NBT premixed were purchased from Sigma-Aldrich, USA. DMSO (99.7%) and MTT reagents were purchased from Alfa Aesar. Anti-PARP monoclonal antibody and anti GAPDH antibody were purchased from Abcam and Santa Cruz Biotechnology, respectively. The human breast cancer cell line (MCF-7), human lung cancer cell line (A549), human ovarian cancer cell line (SKOV3) and Chinese hamster ovary cell line (CHO) were purchased from American Type Culture Collection (ATCC), Manassas, VA. NIH-3T3 cells were obtained from NCCS, Pune.

Stock suspension preparations. The main stock suspensions of **S1–S6** and curcumin (20 mg mL^{-1}) were prepared in DMSO. Freshly prepared stock suspensions were used for all cell culture experiments.

Cell culture experiments. Human lung adenocarcinoma cell line (A549), human breast cancer cell line (MCF-7), human ovarian cancer line (SKOV3), Chinese hamster ovary cell line (CHO) and mouse embryonic fibroblast cell line (NIH-3T3) were maintained in DMEM complete media in a humidified 5% CO_2 incubator at 37 °C.

Cell viability assay. Cell viability assay using MTT reagent is a colorimetric method where the yellow coloured (3-(4,5-di-

methylthiazol-2-yl)-2,5-diphenyl tetrazolium bromide) dye reduces into purple coloured formazan crystals by mitochondrial dehydrogenase enzymes. This assay has been used to determine the cytotoxic nature of drugs. In the present study 10 000 cells per well were seeded into 96 well plates and incubated for 24 hours. Then the cells were treated with different materials in a dose dependent manner (considering the loading of curcumin on the material) for a further 48 hours. All the materials were irradiated under UV light prior to treatment. After 48 hours, 100 μL of MTT reagent (0.5 mg mL^{-1}) was added to each well of the plate by replacing the old media and incubated in the dark for 4 hours. The *in situ* formed formazan dye was then solubilized by DMSO–methanol (1 : 1; v/v) solvent mixture and kept on the shaker for homogeneous mixing for a few minutes. The absorbance of the purple colour dye developed was measured in a micro plate reader (ELx 800 MS) at 570 nm. All the experiments were carried out in triplicate and the results were expressed as normalized viability.

Kinetics of cellular uptake of curcumin loaded mesoporous silicas. In order to understand the cellular uptake efficacy of curcumin loaded mesoporous silicas, a kinetic study was performed. A549 cells were cultured in 24 well plates and treated with **S2**, **S4** and **S6** (10 μM with respect to curcumin). The green fluorescence images were acquired using a Nikon fluorescence microscope (λ_{Ex} = 485 nm; λ_{Em} = 529 nm) after 6 and 12 hours of treatment after thorough washing of cells with DPBS.

Analysis of internalization of curcumin loaded mesoporous silica materials by flow cytometry. To show further evidence of cellular internalization of the curcumin loaded material **S4**, flow cytometry study was carried out in A549 cells. The cells were cultured in 60 mm dishes and incubated with **S4** (10 μM with respect to curcumin) for 12 hours. After trypsinizing the cells, they were fixed in 70% ethanol and washed twice with DPBS. The samples were then analysed in FACScan flow cytometer (BD bioscience) under a FITC channel.

Analysis of cellular internalization of mesoporous silica through ICP-OES. In order to show the cellular internalization of mesoporous silica in cancer cells the ICP-OES method was employed. A549 cells were grown in T75 culture flasks and incubated with all **S1–S6** materials for 6 hours. After the incubation period, the cells were washed thoroughly with DPBS and trypisinized. The total number of cells was counted using a haemocytometer and the cell suspension was digested in nitric acid for 48 hours. The cell digest was submitted for ICP-OES analysis for the assessment of the internalized silica content in A549 cells. The results were expressed as silicon content as nanogram/live cell.

Cell migration inhibition assay. In order to assess the effect of curcumin-loaded mesoporous silica on the cellular migration as well as growth rate inhibition, a cell scratching assay was performed. The cultured A549 monolayer was scratched with the sterile edge of a plastic tip and washed with DPBS for two times. Then the cells were treated with **S4** (10 μM with respect to curcumin) and curcumin (10 μM) for up to 12 hours. The cell migration was analyzed by capturing bright field images of cells for different time periods.

Determination of intracellular superoxide anion radical. The determination of intracellular superoxide anion radical was carried out according to our standard protocol.[14b] In brief, A549 cells (2×10^4 cells per mL) were seeded in a 24 well plate for 24 hours. Then the cells were incubated with **S1–S6** (10 μM with respect to curcumin) and curcumin (10 μM) for a further 48 hours. After that, the cells were washed several times with DPBS and incubated with 10 μM of dihydroethidium (DHE) for 15 minutes in the dark. The cells were again thoroughly washed with DPBS and observed by fluorescence microscopy. The red fluorescence (λ_{Em} = 610 nm) images were collected using a Nikon fluorescence microscope after excitation at λ_{Ex} = 535 nm.

Quantification of ROS through flow cytometry. Intracellular ROS was measured using the flow cytometry technique in A549 cells. The cells were seeded in 60 mm dish until 70% confluent. The cells were then treated with **S1–S6** (10 μM with respect to curcumin) materials and incubated for 24 hours. After that, the cells were washed thoroughly with DPBS 3 times and incubated with DHE fluorescent dye (10 μM) for 15 minutes in the dark. After the incubation period, the cells were thoroughly washed with DPBS to remove the excess dye. All the cells were trypsinized and analyzed under the PE channel in the FACS machine.

Poly ADP ribose polymerase (PARP) analysis by western blotting. Western blot analysis was carried out in A549 cells to analyse the expression of PARP enzyme levels upon treatment with **S3**, **S4** (10 μM with respect to curcumin) and curcumin (10 μM) for 48 hours. The cells were then lysed and proteins were extracted using RIPA (radio immune precipitation assay) buffer solution with a protease inhibitor cocktail. The lysate was centrifuged at 10 000 rpm for 10 minutes at 4 °C and the supernatant obtained was used for the immunoblot procedures. Protein estimation was carried out using the Bradford assay method and equal concentrations of protein samples were loaded in 8% denaturing sodium dodecyl sulfate poly acrylamide gel. After electrophoretic separation of the proteins, they were blotted on the nitrocellulose membrane and blocked in 5% BSA solution for 2 hours. The membrane was incubated with anti-PARP monoclonal primary antibody and anti GAPDH primary antibody in a TBST (Tween-20 (TBS-T; 10 mM Tris, pH 7.5, 150 mM NaCl, 0.05% Tween-20)) solution (dilutions were followed according to manufactures instructions) for 2 hours at room temperature. The membrane was then washed in the TBST solution twice and incubated with the secondary antibody (conjugated with alkaline phosphatase) for 1 hour at room temperature. The blot was developed using the BCIP–NBT solution in the dark.

Analysis of DNA damage by Hoechst-33258–PI double staining. Hoechst-33258 and PI staining dyes were used to analyse the DNA damage induced by **S4** material. A549 cells were cultured in a 24 well plate (10 000 cells per well) and incubated with **S4** (10 μM with respect to curcumin) and curcumin (10 μM) for 24 hours. The cells were then washed and fixed in a 4% formaldehyde solution for 5 minutes and permeabilised with 0.05% triton-X for 10 minutes. A Hoechst-33258–PI stain-

ing solution (containing RNase) was added to the cells and incubated for 30 minutes in the dark. Cells were then washed 3 times with DPBS and observed by fluorescence microscopy. The red fluorescence (λ_{Em} = 610 nm) images were collected using a Nikon fluorescence microscope after excitation at λ_{Ex} = 535 nm. The blue fluorescent images (λ_{Em} = 485 nm) of the Hoechst stained nuclei were obtained after excitation at (λ_{Ex}) at 380 nm.

Results and discussion

Chemistry

Synthesis and amine functionalization of mesoporous silica materials. The curcumin-loaded silica materials were synthesized using KIT-6,[11] MSU-2 [12] and MCM-41 [13] mesoporous silicas as the host materials, according to earlier reports.

Porous materials can usually be impregnated simply in a concentrated solution of the cargo even without functionalization. However, direct impregnation of curcumin on the host materials KIT-6, MSU-2 and MCM-41 under different reaction conditions does not yield high loading contents of curcumin on the materials.

According to previous studies[14a] of the betulinic acid loaded MCM-41 system, the functionalization of the material MCM-41 with amine groups increased the loading content of betulinic acid by the formation of weak intermolecular forces between the amine group of the functionalized materials and the polar groups of betulinic acid.

Additionally, amine functionalized materials have previously been synthesized for a wide range of applications.[15] Following the reported protocols,[14a] the grafting reactions of 3-aminopropyltriethoxysilane (APTES: AP) with the host materials KIT-6, MSU-2 and MCM-41 were carried out to give rise to the amine functionalized materials **S1** (KIT-6-AP), **S3** (MSU-2-AP) and **S5** (MCM-41-AP), respectively (Scheme 1).

Loading of curcumin on amine functionalized mesoporous silica materials. Subsequently, materials **S1**, **S3** and **S5** were refluxed with curcumin in ethanol solvent for 48 hours under nitrogen atmosphere to form curcumin loaded amine functionalized mesoporous silica materials **S2** (KIT-6-AP-CUR), **S4** (MSU-2-AP-CUR)and **S6** (MCM-41-AP-CUR), respectively (in a quantity to give a theoretical 20 wt% ratio) (Scheme 1). These materials were then filtered and dried for 24 hours under vacuum at room temperature. In this case, no washing treatment was carried out to avoid leaching of the adsorbed curcumin.

Characterization of mesoporous silica materials. To confirm the mesoporous properties of the host materials, a nitrogen adsorption–desorption study[16] was first carried out (Table 1). The results showed that the materials KIT-6, MSU-2 and MCM-41 possessed very regular pore diameters of 76.2, 51.1 and 29.6 Å respectively, and a very high BET surface area of 700, 843 and 1117 $m^2\ g^{-1}$, respectively (Table 1). The functionalization of the host materials with aminopropyl groups was identified by the decrease in their pore size and

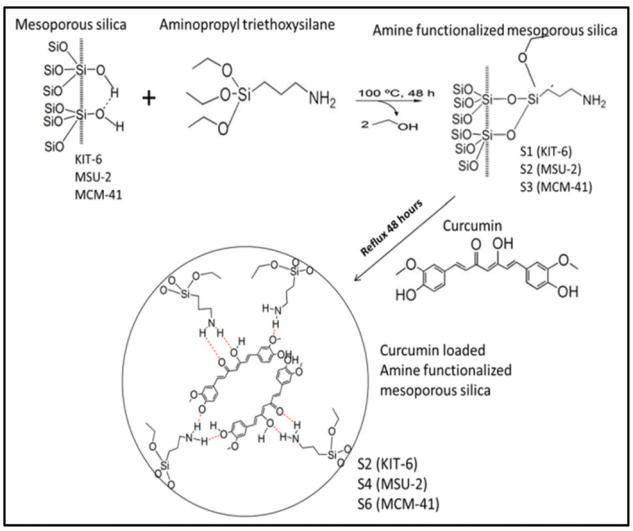

Scheme 1 Synthesis of mesoporous silica based materials **S1–S6**. Amine functionalization of starting materials KIT-6, MSU-2 and MCM-41 with 3-aminopropyltriethoxysilane (APTES) generates **S1**, **S3** and **S5**. The reaction of these materials with curcumin under nitrogen atmosphere forms the curcumin loaded materials **S2**, **S4** and **S6**, respectively.

Table 1 Textural properties of **S1–S6** materials

Materials	Description of materials	S_{BET} ($m^2\ g^{-1}$)	V_p ($cm^3\ g^{-1}$)	d_p (Å)
KIT-6	Mesoporous silica-1	700	0.60	76.2
S1	Functionalized-KIT-6 (KIT-6-AP)	130	0.20	62.5
S2	Curcumin loaded-S1 (KIT-6-AP-CUR)	20	0.04	<18
MSU-2	Mesoporous silica-2	843	0.97	51.1
S3	Functionalized-MSU-2 (MSU-2-AP)	470	0.67	39.5
S4	Curcumin loaded-S3 (MSU-2-AP-CUR)	425	0.49	35.4
MCM-41	Mesoporous silica-3	1117	1.12	29.6
S5	Functionalized-MCM-41 (MCM-41-AP)	650	0.25	18.3
S6	Curcumin loaded-S5 (MCM-41-AP-CUR)	414	0.17	<18

BET area as observed in the nitrogen sorption isotherms of the materials **S1** (Fig. S1†), **S3** (Fig. 1a) and **S5** (Fig. S2†) compared to the corresponding host materials (Table 1).

It is important to mention that the isotherm of material **S1** (Fig. S1†) changes to a type III isotherm after loading with curcumin (**S2**) with a very thin hysteresis loop which is indicative of a microporous or non-porous material, suggesting that physisorption of curcumin may completely block the pores of the system.[11a] It is noteworthy that hysteresis loop in materials **S1** and **S6** was not closed. However, for both materials, the desorption curve is very close to that of the adsorption at very low relative pressures. The very low difference in the desorption step is not significant to be considered as a different behaviour in nitrogen desorption. In addition, after functionalization

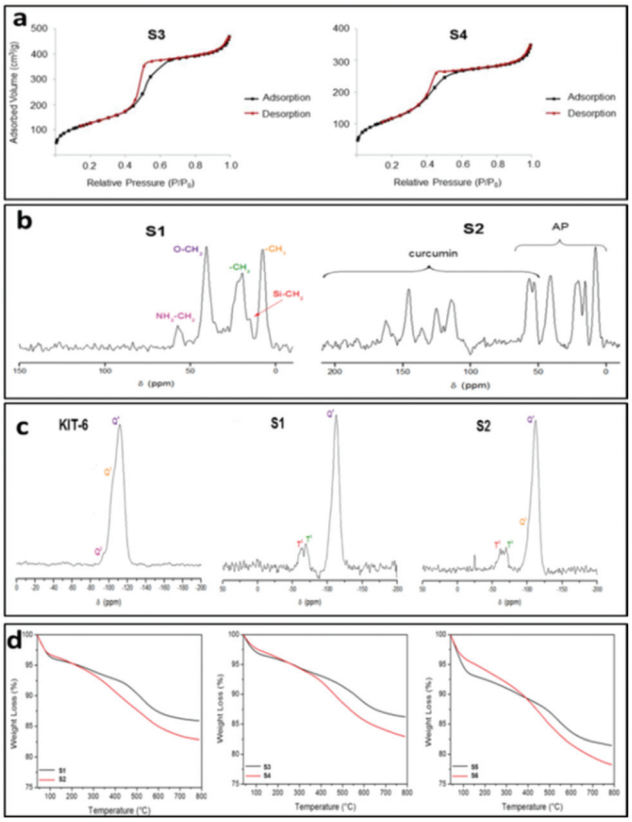

Fig. 1 (a) Nitrogen adsorption–desorption isotherms of materials **S3** and **S4**. (b) ^{13}C-CP MAS NMR spectra of materials **S1** and **S2**. (c) ^{29}Si MAS NMR spectra of materials KIT-6, **S1** and **S2**. (d) Thermogravimetric analysis of materials **S1–S6**.

either with APTS or with curcumin all the materials showed a decrease of the surface area which is higher in ratio in the case of KIT-6-based materials, as is expected due to the higher number of silanol groups in their structure.[11b]

The unmodified KIT-6, MSU-2 and MCM-41 displayed X-ray diffractions (XRD) which were typical for the mesoscopic order of mesoporous materials (Table 2). The result showed a well-resolved pattern at low 2θ with a very sharp diffraction peak for KIT-6, MSU-2 and MCM-41 at 0.9, 1.4 and 2.2°, respectively. These characteristic Bragg's peaks correspond to reflections from the (100) plane in MSU-2 and MCM-41 and the (211) plane in KIT-6. In addition, the MCM-41 diffractogram showed a weak peak at 3.9° which corresponds to reflections from the (110) planes.

Table 2 Interplanar distances, peak positions, size and charge of the materials

Material	*hkl*	2θ (°)	$d_{(100)}$ (Å)	a_0 (Å)	Size (nm)	Charge (mV)
KIT-6	211	0.9	97.3	112.4	—	—
S1	211	0.9	97.0	112.0	5577	−9.36
S2	211	0.9	96.7	111.8	1983	−18.3
MSU-2	100	1.4	62.1	71.7	—	—
S3	100	1.3	68.1	78.6	3781	−0.799
S4	100	1.3	66.2	76.5	1915	7.16
MCM-41	100	2.2	39.5	45.6	—	—
S5	100	2.4	37.2	42.9	2124	12.3
S6	100	2.3	37.9	43.9	1233	−23.2

A significant decrease in the intensity of the diffraction peaks was also observed after the loading of curcumin compared to the amine functionalized materials. This is due to the blocking of the dispersion centres by the organic fragment (AP and/or curcumin) for diffractograms of mesoporous silica materials (Fig. S3–S6†).

The incorporation of the 3-aminopropyl group was also confirmed by multinuclear MAS NMR spectroscopy. The ^{13}C-CP MAS NMR spectrum of **S1** (Fig. 1c) showed a set of five signals between *ca.* 10 and 60 ppm corresponding to the three carbon atoms of the methylene groups of the alkyl chain of AP along with two intense signals corresponding to the carbon atoms of the ethoxy moieties. On the other hand, the ^{13}C-CP MAS NMR spectrum of the curcumin loaded material **S2** (Fig. 1c) showed the appearance of two new broad signals of low intensity at around 50 ppm, corresponding to the methoxy carbon atoms of the curcumin and a set of new signals between 100 and 200 ppm assigned to the sp^2 carbon atoms (aromatic and carbonyl) of the molecule. Similar results could be anticipated for the other set of materials (**S3–S4**; **S5–S6**).

The amine-functionalization of silica materials was confirmed by ^{29}Si MAS NMR spectroscopy. The mesoporous silica materials exhibit typical Q^2, Q^3 and Q^4 peaks in the ^{29}Si MAS NMR spectra[17] as observed in the case of host material KIT-6 (Fig. 1b).

On the other hand, the ^{29}Si MAS NMR spectrum of **S1** (Fig. 1b) showed a substantial decrease in the intensity of Q^2 and Q^3 sites in comparison to that of the host material KIT-6. The spectra of **S1** also exhibited the appearance of two additional peaks of low intensity at *ca.* −55 and −66 ppm corresponding to the T^2 ($(SiO)_2SiOH$-R) and T^3 ($(SiO)_3Si$-R) sites, respectively, which come from the functionalization with the 3-aminopropyltriethoxysilane. Further, the curcumin loaded material **S2** (Fig. 1b) showed slight differences in their ^{29}Si MAS NMR spectra compared to the spectrum of **S1** (Fig. 1b). Similar results could be expected for the other set of materials (MSU-2, **S3** and **S4**; MCM-41, **S5** and **S6**, see Fig. S7 and S8†). The results altogether suggest an amine functionalization in the corresponding host materials.

In the FT-IR spectra of **S2**, **S4** and **S6** some typical bands corresponding to the curcumin loading were observed with special importance at *ca.* 1520 cm^{-1}, which can be attributed to the carbonyl groups of curcumin (Fig. S9–S11†).

The quantity of organic groups attached to the material was determined by TGA and elemental analysis leading to an amine functionalization of 9.1, 8.5 and 11.0 wt% for the materials **S1**, **S3** and **S5**, respectively (Table 3). Furthermore, in order to determine the N%, an elemental analysis was carried out on the materials **S1**, **S3** and **S5** (Table S1,† Fig. 1d and S12†). Analyzing the elemental analyses data, it was found that the experimental and calculated N% are very similar to the functionalization rates (in mmol of compound per gram of material and in wt%). However, the C% showed that the

Table 3 Curcumin content measured by TGA

Material	% weight loss (20–100 °C)	% weight loss (100–600 °C)	% curcumin
S1	3.62	9.08	—
S2	3.28	11.76	2.68
S3	2.93	8.46	—
S4	2.32	14.34	3.56
S5	5.31	11.00	—
S6	3.75	14.58	3.58

functionalization reaction of APTES occurred through the elimination of only two ethanol molecules while one ethoxy group was retained on the supported amino ligand (Scheme 1). The TGA and elemental analysis results also showed that the loading contents of curcumin in **S2**, **S4** and **S6** materials were *ca.* 2.7, 3.6 and 3.6%, respectively (Table 3, Fig. 1d and S12†). Thus, the encapsulation efficiency of each of the studied materials **S2**, **S4** and **S6** were found to be 13.4, 17.8 and 17.9%, respectively.

Finally, the mesoporous silica based materials were characterized by SEM and TEM. The SEM image of KIT-6 showed that this material (solid state) does not a well-defined particle shape and forms aggregates of microns (5.4 ± 2.2 μm) while the SEM image of MCM-41 showed that it consists of hexagonal or quasi-spherical particles of size *ca.* 700 nm (708 ± 157 nm) (Fig. S13†). On the other hand, the particle size of MSU-2 is found to be 439 ± 97 nm, as observed from the SEM images (calculated using Image J analyzing software) of the material (Fig. S13†).

The TEM images of KIT-6 and MCM-41 show the ordered arrangements of the pores while in the case of MSU-2 a disordered arrangement of the pores was observed (Fig. S14†). The curcumin loaded materials **S2**, **S4** and **S6** were also characterized by SEM and TEM, which showed that they maintained their original morphology, particle size and arrangement, and pore distribution (Fig. 2) with respect to the host materials KIT-6, MSU-2 and MCM-41. Additionally, a dynamic light scattering (DLS) study was carried out with all **S1–S6** materials and the results are shown in Table 2 and in Fig. S15–S20.†

Release kinetic study of curcumin from curcumin loaded silica materials. The release kinetic study of curcumin was carried out in a blood simulated fluid (Tris-HCl: pH7.4). The curcumin-loaded materials **S2**, **S4** and **S6** were incubated in Tris-HCl buffer at 37 °C up to different time points. The incubated solutions were then filtered and the content of curcumin present in the filtrate was determined using UV-visible spectroscopy (see Experimental section).

The results suggested that the release of curcumin was higher in the case of **S6** compared to that of **S2** and **S4** (Fig. 3). It was observed that **S6** released 1.8 ppm curcumin at pH 7.4 (corresponding to 2.3 wt% loaded curcumin) after 240 hours. On the other hand, materials **S2** and **S4** released less quantity of curcumin (0.4 and 0.8 ppm corresponding to 0.8 and 1.1 wt% of the loaded curcumin, respectively) into the studied medium after 240 hours. In a direct comparison between materials **S6** with the other curcumin loaded materials (**S2** and **S4**), **S6** seems to present a slightly faster release which might be a consequence of the higher loading of curcumin in the external surface area of **S6** compared to that of **S2** and **S4**.

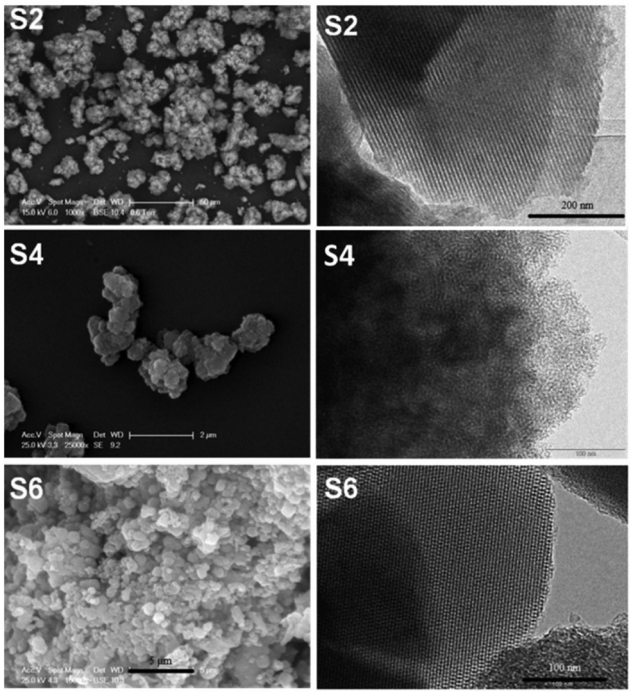

Fig. 2 Electron microscopy images of materials **S2**, **S4** and **S6**. The SEM images show that the morphology and arrangement of the materials are maintained as in the corresponding starting materials. TEM images exhibit pore arrangements of the materials similar to those found in the starting materials.

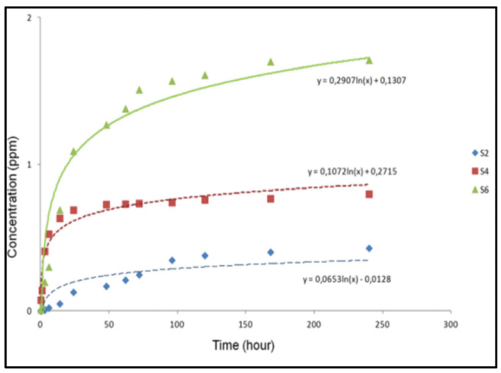

Fig. 3 Release study of curcumin present in **S2**, **S4** and **S6** in Tris-HCl (pH 7.4). The results show the slow and sustained release of curcumin from the materials. The error bars are omitted for clarity.

Biology

Cell viability assay (MTT assay). MTT assay is a well-established method to evaluate the *in vitro* cytotoxicity of materials.[18] It is well known that mesoporous silica materials

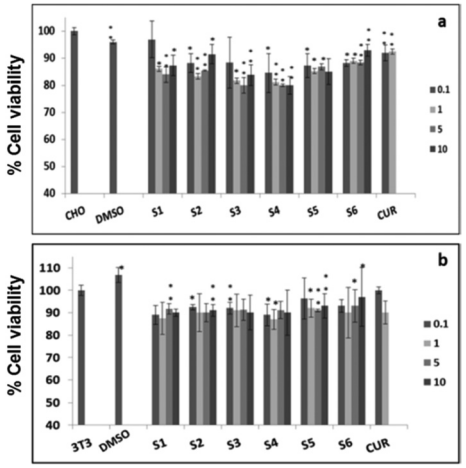

Fig. 4 Cell viability assay in normal cells (CHO and NIH-3T3) using MTT reagent. This study shows that all the materials including curcumin do not inhibit the viability of non-cancerous CHO (a) and NIH-3T3 (b) cells, suggesting their biocompatible nature. Numerical values represent the concentration of the silica materials in μM (with respect to curcumin). $*P \leq 0.05$, $**P \leq 0.005$ compared to control.

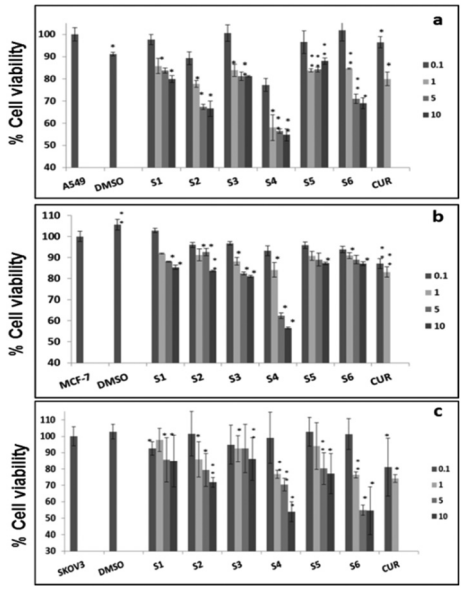

Fig. 5 Cell viability assay in cancer cells (A549, MCF-7 and SKOV3) using MTT reagent. All the curcumin loaded silica nanomaterials (especially **S4**) show better cytotoxic responses compared to that of free curcumin in A549 (a), MCF-7 (b) and SKOV3 (c) cancer cells. Free curcumin (1 and 10 μM) and DMSO have been used as the positive control and vehicle control experiment, respectively. Numerical values represent the concentration of the silica materials in μM (with respect to curcumin). $*P \leq 0.05$, $**P \leq 0.005$ compared to control.

are biocompatible in normal cells.[19] The cytotoxicity profiles of materials **S1–S6** (0.1–10 μM with respect to curcumin) were analysed in CHO (Fig. 4a) and NIH-3T3 (Fig. 4b) normal cell lines employing the MTT assay. The results demonstrated that the viability of the normal cells was not affected in the presence of the materials, indicating their biocompatible nature.

Further, cell viability assay was also carried out in different cancer cell lines, such as A549, MCF-7 and SKOV3. The results showed that all the curcumin loaded materials (**S2**, **S4** and **S6**) were cytotoxic in A549 (Fig. 5a) and SKOV3 (Fig. 5b) cells compared to the free curcumin. However, only the **S4** material showed significant cytotoxicity in MCF-7 cells (Fig. 5c), which may be due to the enhanced uptake of **S4** in cancer cells compared to other curcumin loaded materials (**S2** and **S6**). The amine functionalized mesoporous silica materials (**S1**, **S3** and **S5**) also exhibited a slight cytotoxicity in the respective cancer cell lines, which may be due to the functionalization effect which corroborates the earlier reports.[20]

It has previously been reported that curcumin demonstrates a dual nature to be both a neuroregenerative agent in endogenous neural stem cells (NSC)[21] as well as a cytotoxic agent in cancer cells,[22] demonstrating its versatile properties in different cell types. Similarly, in the present study, the results indicated that the curcumin present in the mesoporous materials (**S2**, **S4** and **S6**) were biocompatible in normal cells and cytotoxic in cancer cells. Our results have further been evidenced by an earlier study[23] that showed a greater curcumin uptake in cancer cells compared to normal NIH 3T3 cells, which may be the reason for the biocompatibility of curcumin present in mesoporous materials in normal cells and its cytotoxicity in cancer cells. These results altogether suggest that the curcumin loaded materials, especially **S4**, enhance the bioavailability of curcumin by partially overcoming the problems associated with the low systematic bioavailability of curcumin originating from its low solubility and instability, indicating the future potential application of mesoporous silica materials as curcumin drug delivery vehicles in cancer treatments.[24]

Cellular internalization of curcumin loaded silica materials. A cellular uptake study was carried out to determine the internalization of the curcumin loaded materials in cancer cells. The green fluorescence property of curcumin was used to observe the cellular entry of curcumin loaded mesoporous silicas in A549 cells. The cells were incubated with the curcumin loaded materials along with free curcumin for different periods of time (6 hours and 12 hours). The results exhibited that the untreated control cells and cells treated with free curcumin did not show any green fluorescence (Fig. 6). On the other hand, the cells treated with curcumin loaded materials (**S2**, **S4** and **S6**) exhibited green fluorescence indicating a cellular uptake of the materials. Additionally, the fluorescence intensity increases from 6 hours to 12 hours of incubation of **S2**, **S4** and **S6**, indicating that their cellular internalization increased in a time dependent manner. Interestingly, **S4** treated cells showed a higher green fluorescence intensity than the cells treated with **S2** or **S6** suggesting a higher uptake of **S4** materials in cancer cells (Fig. 6 and S21†). These results corroborate the cell viability data showing the better cytotoxic efficacy of **S4** in cancer cells than that of other curcumin loaded materials. According to the earlier report, it seems that the cellular uptake of the materials may happen through

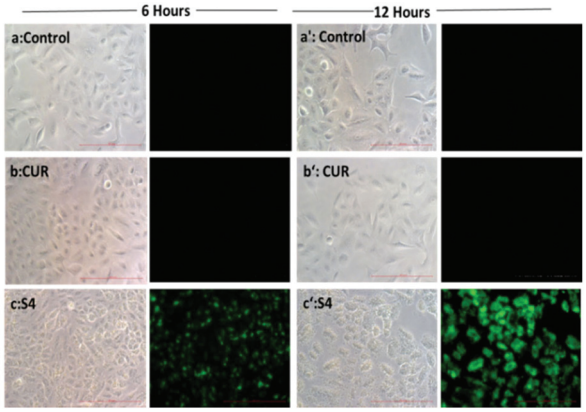

Fig. 6 Kinetics of cellular internalization of curcumin loaded mesoporous silica in A549 cells. Results show that the internalization of **S4** increases in a time dependent manner (6 hours–12 hours). Row 1: untreated A549 cells (a: 6 hours, a': 12 hours), row 2: cells treated with curcumin (CUR: 10 μM; b: 6 hours, b': 12 hours), row 3: cells treated with **S4** (10 μM w.r.t. CUR; c: 6 hours, c': 12 hours). From left to right, column 1 and 2 are the bright field and fluorescent images after a 6 hour treatment, whereas column 3 and 4 are the bright field and fluorescent images after a 12 hour treatment. Scale bar = 200 micron.

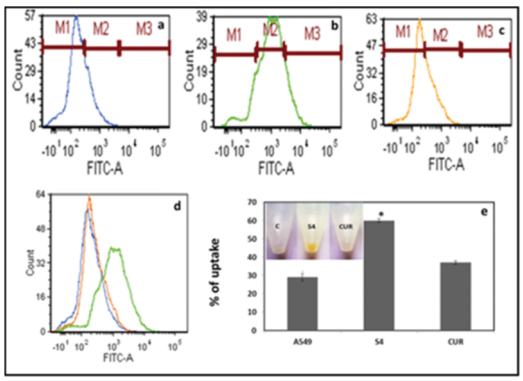

Fig. 7 Flow cytometry analysis for the cellular uptake of **S4** in A549 cells. The green fluorescence property of curcumin was utilized to study the cellular entry of **S4** materials. In the FITC channel the **S4** material shows more transfection after 12 hours of treatment compared to free curcumin. a: control untreated A549 cells, b: cells treated with **S4** (10 μM w.r.t. CUR), c: cells treated with CUR (10 μM), d: merged image of a, b and c histograms. e: Quantification of % cellular uptake, represented as a histogram. The inset figure shows the curcumin uptake (yellow colour) in the cell pellet. $*P \leq 0.05$, $**P \leq 0.005$ compared to control.

macro pinocytosis.[25] However, the exact mechanism of cellular internalization of these materials is not quite clear and requires an in depth investigation which is beyond the scope of this present study.

Quantification of cellular uptake by flow cytometry. Curcumin uptake through mesoporous silica materials in A549 cells was quantified using flow cytometry. The cells treated with the **S4** material showed a significant shift of the fluorescence peak in the FITC channel compared to untreated cells and cells treated with free curcumin indicating a higher uptake of curcumin in the form of **S4** (Fig. 7a–d).

The quantification results also showed that the cellular uptake of curcumin present in **S4** (60%) was greater compared to free curcumin (37%) at a similar dose (Fig. 7e). The flow cytometry results also corroborate with the fluorescence microscopy data for cellular internalization of **S4**.

Cellular uptake of mesoporous silica materials. The biological influence of functional materials or nanoparticles depends on cellular internalization. We carried out cellular uptake studies of the materials in the A549 cell line to confirm their internalization through the ICP-OES technique (Fig. S22†). The result showed that all the mesoporous materials (**S1–S6**) internalized inside A549 cells after an incubation of 6 hours even though the materials are micro sized (see Table 2).

Interestingly, the maximum cellular uptake was observed for **S4** materials which may be evidence of its more cytotoxic nature in different cancer cells. The exact mechanism of cellular uptake of the materials is quite unclear and a thorough investigation is still required, which is beyond the scope of the present study. However it can be assumed that the microsized mesoporous silica materials (>1 μm) may internalize through macro pinocytosis as reported in an earlier study.[25]

Cell migration inhibition assay. Cell migration inhibition assay was performed in A549 cells to analyse the influence of curcumin present in mesoporous silica materials on the migration of cancer cells. The results showed that the untreated control cells migrated rapidly toward the scratched area. However, the wound area remained practically unchanged in cells treated with curcumin loaded materials (**S2**, **S4** and **S6**) indicating the inhibition of cancer cell migration in the presence of those materials (Fig. 8a–d). The wound area at different time points (0 hour and 12 hours) was calculated using Image J software (Fig. 8e). The inhibition of cancer cell migration confirms that the curcumin delivery through mesoporous silica influences the growth rate of cancer cells leading to the inhibition of metastasis.

Determination of cellular superoxide ion radical. Superoxide ion radical is a reactive oxygen species which can interfere with mitochondrial function.[26] It has been reported that curcumin can produce intracellular superoxide ion radicals which may be one of the reasons for its anticancer activity.[27] In present study, the presence of an intracellular superoxide ion radical was determined using the dihydroethidium (DHE) reagent. Fig. 9 shows that untreated control A549 cells did not exhibit any red fluorescence, while cells treated with curcumin and curcumin loaded materials **S2** and **S6** showed a slight red fluorescence, indicating the generation of intracellular super oxide ion radical in lesser amount.

However, **S4** treated cells exhibited a significant intense red fluorescence suggesting the excessive formation of the superoxide ion radical. The results corroborate with the internalization and cell viability data revealing the higher uptake of **S4** which produced excessive amount of ROS leading to enhanced cytotoxicity in cancer cells.

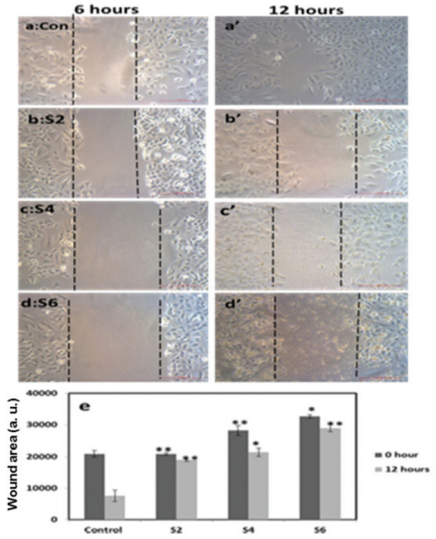

Fig. 8 Cell migration inhibition study of curcumin loaded materials in A549 cells. All the curcumin loaded materials **S2**, **S4** and **S6** (10 μM w.r.t curcumin) show the inhibition of cell migration compared to untreated control cells after 12 hours of treatment. (a–d): 0 hour treatment for control, **S2**, **S4** and **S6** respectively. (a′–d′): 12 hours treatment for control, **S2**, **S4** and **S6** respectively. Scale bar = 200 micron. (e): the quantification of the wound area suggests that the wound remained almost unaltered in cells treated with curcumin loaded materials (**S2**, **S4** and **S6**) compared to the untreated cells. $*P \leq 0.05$, $**P \leq 0.005$ compared to control.

Quantification of cellular ROS. The intracellular formation of superoxide anion radical in control untreated A549 cells and cells treated with materials **S1–S6** was quantitatively measured through flow cytometry using the DHE reagent (Fig. 10). The results revealed that the **S4** material showed a shift of the peak of cellular fluorescence compared to control untreated cells and cells treated with other materials, indicating a significant enhancement of intracellular ROS in presence of **S4**. This study further supports the generation of excessive intracellular ROS in presence of **S4**.

Analysis of PARP expression by immunoblotting. Poly ADP ribose polymerase, a DNA repairing enzyme, protects cells from DNA damage. Li *et al.* showed that down regulation of PARP enzyme levels in glioma cells activates apoptosis protein expression.[28] In the present study, immunoblot analysis in A549 cells revealed that the cells treated with **S4** showed the down regulation of PARP enzyme levels compared to untreated control cells and cells treated with free curcumin as well as the corresponding amine functionalized material **S3** (Fig. 11). The results altogether suggested that the curcumin loaded **S4** material induced cytotoxicity in A549 cancer cells through apoptosis.

Analysis of apoptosis by Hoechst-33258–PI staining. DNA damage is one of the major incidents that take place during apoptosis.[29] During the late phase of apoptosis, the cells contain damaged DNA which binds more with nuclear stains.

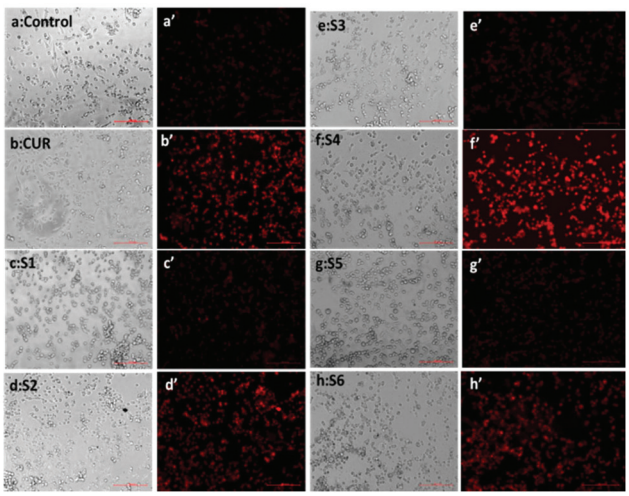

Fig. 9 Determination of intracellular superoxide anion radicals in A549 cells by fluorescence microscopy. The results show the formation of the superoxide ion radical in cells treated with curcumin loaded materials. Phase images (a–h) and corresponding fluorescent images (a′–h′) of A549 cells. a–a′: untreated control cells; b–b′: cells treated with curcumin (10 μM); c–c′: cells treated with **S1**; d–d′: cells treated with **S2**; e–e′: cells treated with **S3**; f–f′: cells treated with **S4**; g–g′: cells treated with of **S5**; h–h′: cells treated with **S6**. The doses of all curcumin loaded silica materials are 10 μM w.r.t. curcumin. Scale bar = 200 micron.

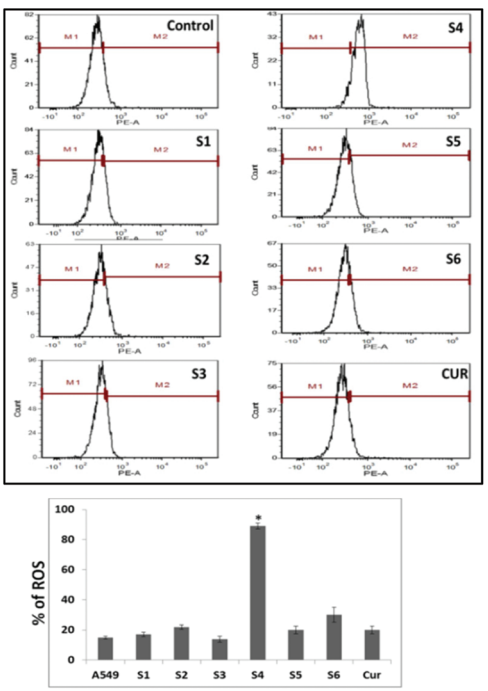

Fig. 10 Quantification of intracellular ROS in A549 cells by flow cytometry. **S4** material shows the red colour fluorescence as evidenced by the shift of the peak compared to control cells. The quantification of the generation of ROS in presence of different materials is presented in the histogram. $*P \leq 0.05$, $**P \leq 0.005$ compared to control.

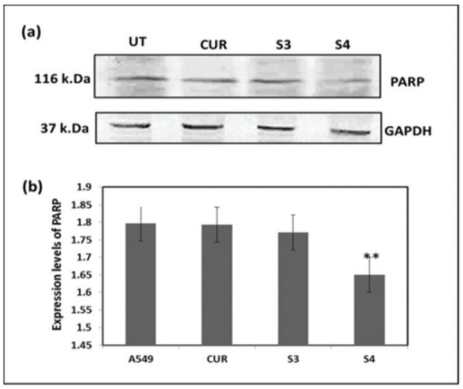

Fig. 11 Western blot analysis for poly ADP ribose polymerase (PARP) expression in A549 cells. (a) Immunoblotting shows the down regulation of the PARP levels in cells treated with **S4** compared to untreated control cells, indicating the induction of apoptosis by the material. (b) The quantification of PARP expression with respect to GAPDH is presented as a histogram. $*P \leq 0.05$, $**P \leq 0.005$ compared to control.

Hence, Hoechst-33258–PI staining was performed according to earlier literature[30] in order to analyze the apoptosis induced by the curcumin loaded material **S4**. The results showed that the untreated cells and cells treated with free curcumin exhibited poor red fluorescence. However the cells treated with **S4** showed a brighter red fluorescence, indicating major DNA damage in A549 cells which leads to apoptosis (Fig. 12). The results also correlate with the western blot analysis data which suggests that the down regulation of PARP causes the DNA damage.

The overall cytotoxic mechanism of curcumin in the mesoporous silica material is presented in Scheme 2. The curcumin loaded mesoporous materials enhance the uptake of curcumin in cancer cells. The generation of the intracellular superoxide ion radical by the internalized curcumin present in the silica materials causes the oxidative stress in cancer cells which subsequently leads to PARP down regulation and DNA damage. The overall mechanism suggests that cancer cell death is through the activation of apoptosis.

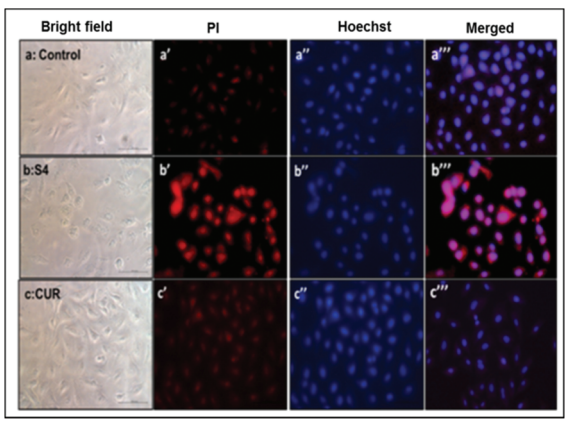

Fig. 12 Analysis of apoptosis by Hoechst–PI staining in A549 cells. Row 1 (a–a′′): control untreated cells, row 2 (b–b′′): cells treated with **S4** (10 μM w.r.t curcumin) and row 3 (c–c′′): cells treated with curcumin (CUR: 10 μM). From left to right, column 1: bright field image, column 2: red fluorescence of PI, column 3: blue fluorescence images for Hoechst 33258 stained nuclei and column 4: merged images of corresponding treatment sets. **S4** treated A549 cells show red fluorescence with a higher intensity compared to untreated control cells, indicating the induction of apoptosis. Scale bar = 100 micron.

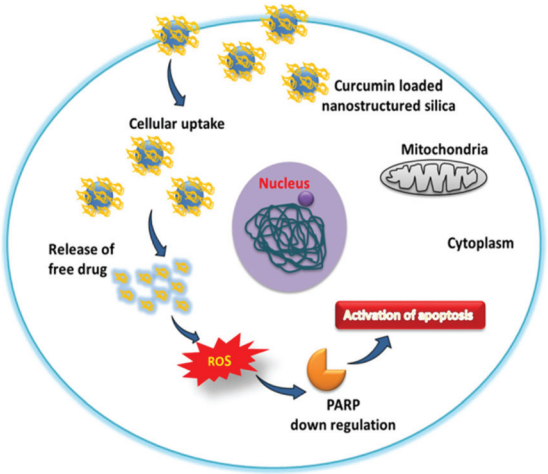

Scheme 2 Anticancer mechanism of curcumin loaded mesoporous silica materials. The curcumin loaded silica materials after being internalized into the cancer cells, release curcumin into the cytoplasm. Then the released curcumin induces the formation of intracellular reactive oxygen species leading to the down regulation of DNA repairing enzyme PARP, which ultimately causes cellular death through the activation of apoptosis.

Conclusions

We have prepared a series of curcumin loaded mesoporous silica materials which have been thoroughly characterized by different physico-chemical methods. Release kinetic studies with the materials reveal the slow and sustained release of curcumin at physiological pH (7.4). Furthermore, *in vitro* studies demonstrate that all the curcumin loaded materials, especially **S4**, show the inhibition of cancer cell viability and migration compared to free curcumin, suggesting the efficacy of the drug delivery system. The intracellular production of reactive oxygen species (ROS), especially $O_2^{\bullet -}$, and the down regulation of PARP are the molecular mechanisms behind the anti-cancer activity of the curcumin loaded materials. This study demonstrates the future potential application of curcumin loaded silica based mesoporous materials for the treatment of cancer diseases.

Acknowledgements

We gratefully acknowledge financial support from the Ministerio de Economía y Competitividad, Spain (Grant no. CTQ-2012-30762). C. Corpa, S. García, E. Hernández and

D. Pérez are gratefully acknowledged for helpful discussions. CRP is grateful to DST, New Delhi for 'Ramanujan Fellowship grant' (SR/S2/RJN-04/2010; GAP0305) and CSIR, New Delhi for generous financial support from 12th Five Year Plan (FYP) projects (CSC0302 and CSC0111) for this research. AKB is thankful to UGC, New Delhi for senior research fellowship. We are thankful to analytical chemistry division (CSIR-IICT) for helping in the detection of metal content in biological samples by ICPOES technique.

References

1 H. Zhou, C. S. Beevers and S. Huang, *Curr. Drug Targets*, 2011, **12**, 332.
2 E. J. Seo, V. Kuete, O. Kadioglu, B. Krusche, S. Schroder, H. J. Greten, J. Arend, I. S. Lee and T. Efferth, *eCAM*, 2013, 131306.
3 R. K. Maheshwari, A. K. Singh, J. Gaddipati and R. C. Srimal, *Life Sci.*, 2006, **78**, 2081.
4 Y. Son, J. H. Lee, Y. K. Cheong, H. T. Chung and H. O. Pae, *BioMed Res. Int.*, 2013, 918039.
5 H. Hatcher, R. Planalp, J. Cho, F. M. Torti and S. V. Torti, *Cell. Mol. Life Sci.*, 2008, **65**, 1631.
6 (*a*) G. Bar-Sela, R. Epelbaum and M. Schaffer, *Curr. Med. Chem.*, 2010, **17**, 190; (*b*) T. Tanaka, *J. Carcinog.*, 2009, **8**, 5; (*c*) D. Bandyopadhyay, *Front. Chem.*, 2014, **2**, 113; (*d*) J. L. Yang and W. Zhang, *Curr. Opin. Oncol.*, 2013, **25**, 398; (*e*) S. S. Dhule, P. Penfornis, T. Frazier, R. Walker, J. Feldman, G. Tan, J. B. He, A. Alb, V. John and R. Pochampally, *Nanomed.: Nanotechnol., Biol. Med.*, 2012, **8**, 440; (*f*) A. Luetke, P. A. Meyers, I. Lewis and H. Juergens, *Cancer Treat. Rev.*, 2014, **40**, 523.
7 V. S. Gota, G. B. Maru, T. G. Soni, T. R. Gandhi, N. Kochar and M. G. Agarwal, *J. Agric. Food Chem.*, 2010, **58**, 2095.
8 (*a*) L. Mamani, S. Nikzad, H. Kheiri-Manjili, S. Al-Musawi, M. Saeedi, S. Askarlou, A. Foroumadi and A. Shafiee, *Eur. J. Med. Chem.*, 2014, **83**, 646; (*b*) S. Kim, M.-J. Stebe, J.-L. Blin and A. Pasc, *J. Mater. Chem. B*, 2014, **2**, 7910.
9 N. Rocks, S. Bekaert, I. Coia, G. Paulissen, M. Gueders, B. Evrard, J. C. Van Heugen, P. Chiap, J. M. Foidart, A. Noel and D. Cataldo, *Br. J. Cancer*, 2012, **107**, 1083.
10 (*a*) Y. M. Tsai, W. L. Chang-Liao, C. F. Chien, L. C. Lin and T. H. Tsai, *Int. J. Nanomed.*, 2012, **7**, 2957; (*b*) O. Naksuriya, S. Okonogi, R. M. Schiffelers and W. E. Hennink, *Biomaterials*, 2014, **35**, 3365; (*c*) A. Baeza, M. Colilla and M. Vallet-Regí, *Expert Opin. Drug Delivery*, 2015, **12**, 319; (*d*) Y. Wang, Q. Zhao, N. Han, L. Bai, J. Li, J. Liu, E. Che, L. Hu, Q. Zhang, T. Jiang and S. Wang, *Nanomed.: Nanotechnol., Biol. Med.*, 2015, **11**, 313; (*e*) J. Safari and Z. Zarnegar, *J. Saudi Chem. Soc.*, 2014, **18**, 85.
11 (*a*) P. J. Lebed, K. de Souza, F. Bilodeau, D. Lariviere and F. Kleitz, *Chem. Commun.*, 2011, **47**, 11525; (*b*) F. Kleitz, S. Hei Choi and R. Ryoo, *Chem. Commun.*, 2003, 2136–2137.
12 D. Perez-Quintanilla, A. Sanchez, I. del Hierro, M. Fajardo and I. Sierra, *J. Nanosci. Nanotechnol.*, 2009, **9**, 4901.
13 M. V. Landau, S. P. Varkey, M. Herskowitz, O. Regev, S. Pevzner, T. Sen and Z. Luz, *Microporous Mesoporous Mater.*, 1999, **33**, 149.
14 (*a*) S. Sanchez-Munoz, S. Gomez-Ruiz, D. Perez-Quintanilla, S. Morante-Zarcero, I. Sierra, S. Prashar, R. Paschke and G. N. Kaluderovic, *ChemMedChem*, 2012, **7**, 670; (*b*) S. Mukherjee, D. Chowdhury, R. Kotcherlakota, S. Patra, B. Vinothkumar, M. P. Bhadra, B. Sreedhar and C. R. Patra, *Theranostics*, 2014, **4**, 316.
15 M. Vallet-Regi, F. Balas and D. Arcos, *Angew. Chem., Int. Ed.*, 2007, **46**, 7548.
16 K. S. W. Sing, D. H. Everett, R. Haul, L. Moscou, R. A. Pierotti, J. Rouquerol and T. Siemieniewska, *Pure Appl. Chem.*, 1985, **57**, 603.
17 G. Engelhardt and D. Michel, *High Resolution Solid-State NMR of Silicate and Zeolites*, Wiley-Blackwell, 1987.
18 S. Mukherje, P. Sriram, A. K. Barui, S. K. Nethi, V. Veeriah, S. Chatterjee, K. I. Suresh and C. R. Patra, *Adv. Healthcare Mater.*, 2015, **4**, 1722.
19 (*a*) J. Ceballos-Torres, S. Prashar, M. Fajardo, A. Chicca, J. Gertsch, A. B. Pinar and S. Gómez-Ruiz, *Organometallics*, 2015, **34**, 2522; (*b*) G. N. Kaluđerović, D. Pérez-Quintanilla, I. Sierra, S. Prashar, I. del Hierro, Ž. Žižak, Z. D. Juranić, M. Fajardo and S. Gómez-Ruiz, *J. Mater. Chem.*, 2010, **20**, 806; (*c*) A. Balbín, F. Gaballo, J. Ceballos-Torres, S. Prashar, M. Fajardo, G. N. Kaluderovic and S. Gómez-Ruiz, *RSC Adv.*, 2014, **4**, 54775.
20 (*a*) A. J. Di Pasqua, K. K. Sharma, Y.-L. Shi, B. B. Toms, W. Ouellette, J. C. Dabrowiak and T. Asefa, *J. Inorg. Biochem.*, 2008, **102**, 1416; (*b*) Z. Tao, B. B. Toms, J. Goodisman and T. Asefa, *Chem. Res. Toxicol.*, 2009, **22**, 1869; (*c*) Y. Sanchez, G. P. Simon, E. Calvino, E. de Blas and P. Aller, *J. Pharmacol. Exp. Ther.*, 2010, **335**, 114.
21 S. K. Tiwari, S. Agarwal, B. Seth, A. Yadav, S. Nair, P. Bhatnagar, M. Karmakar, M. Kumari, L. K. Chauhan, D. K. Patel, V. Srivastava, D. Singh, S. K. Gupta, A. Tripathi, R. K. Chaturvedi and K. C. Gupta, *ACS Nano*, 2014, **8**, 76.
22 M. A. Khan, S. Gahlot and S. Majumdar, *Mol. Cancer Ther.*, 2012, **11**, 1873.
23 K. K. Gupta, S. S. Bharne, K. Rathinasamy, N. R. Naik and D. Panda, *FEBS J.*, 2006, **273**, 5320.
24 Z. Tao, B. B. Toms, J. Goodisman and T. Asefa, *Chem. Res. Toxicol.*, 2009, **22**, 1869.
25 R. A. Petros and J. M. DeSimone, *Nat. Rev. Drug Discovery*, 2010, **9**, 615.
26 D. F. Stoweand and A. K. S. Camara, *Antioxid. Redox Signaling*, 2009, **11**, 1373.
27 J. Cao, L. Jia, H. M. Zhou, Y. Liu and L. F. Zhong, *Toxicol. Sci.*, 2006, **91**, 476.
28 B. Li, H. He, B. B. Tao, Z. Y. Zhao, G. H. Hu, C. Luo, J. X. Chen, X. H. Ding, P. Sheng, Y. Dong, L. Zhang and Y.-C. Lu, *Oncol. Lett.*, 2012, **28**, 909.
29 W. P. Roos and B. Kaina, *Mol. Med.*, 2006, **12**, 440.
30 C. Riccardi and I. Nicoletti, *Nat. Protoc.*, 2006, **1**, 1458.